Available online at www.sciencedirect.com
ScienceDirect
ELSEVIER
JOURNAL OF RARE EARTHS, Vol. 30, No. 10, Oct. 2012, P. 972
JOURNAL OF RARE EARTHS
www.re-journal.com/en/

Investigations into thermoluminescence and afterglow characterization of strontium aluminates with boron-modification and reductions via sol-gel route

I-Cherng Chen (陈一诚)[1], Ker-Kong Chen (陈克恭)[2], Hong-Sen Chen (陈弘森)[2], Je-kang Du (杜哲光)[2], Tsao-Jen Lin (林昭任)[3], Shiu-Shiung Lin (林秀雄)[4], Teng-Ming Chen (陈登铭)[5], Tien-Yu Shieh (谢天渝)[2]

(1. Material Applications Center/IS, Industrial Technology Research Institute, Tainan 709, Taiwan, China; 2. College of Dental Medicine, Kaohsiung Medical University, Kaohsiung 807, Taiwan, China; 3. Chemical Engineering Department, National Chung-Cheng University, Chia-Yi 621, Taiwan, China; 4. Orthodontic Division, Department of Dentistry, Kaohsiung Chang Gung Memorial Hospital and Chang Gung University College of Medicine, Kaohsiung 833, Taiwan, China; 5. Applied Chemistry Department, National Chiao Tung University, Hsinchu 30050, Taiwan, China)

Received 28 March 2011; revised 18 April 2011

Abstract: The effects of strontium aluminates of $SrAl_2O_4:Eu^{2+},Dy^{3+}$ (SAED) and boron-modified SAED (BSAED) phases synthesized from a sol-gel process on thermoluminescence (TL) along with their afterglow properties were systematically investigated with thermal activation in the different atmospheres. The result showed that the addition of boron and the reduction routes of Eu^{3+} to Eu^{2+} in $SrAl_2O_4:Dy^{3+}$ were related to phosphorescent decay properties. The aid of Dy^{3+} to induce the hole-trapping effect required both SAED and BSAED to be heated at 1300 °C under the H_2/N_2 (5%:95%) atmosphere. However, the trapping behavior of the reductions of SAED in nitrogen was similar to the compound without Dy^{3+} co-doping $SrAl_2O_4:Eu^{2+}$ (SAE) in H_2/N_2 (5%:95%). BSAED showed deeper traps *in situ* compared to SAED which contained no boron, and this led to the better afterglow properties of BSAED than those of SAED. The afterglow spectrum of BSAED showed two peaks at 400±1 nm and 485±1 nm, which were two individuals composed and contributed from different depths of traps at 0.57 and 0.76 eV, accordingly. The depth of the traps was calculated from the Hoogenstraaten's plot of glow curves. The calculations for SAED and SAE were at around 0.43 and 0.18 eV, respectively.

Keywords: $SrAl_2O_4:Eu^{2+},Dy^{3+}$; boron addition; long afterglow; thermoluminescence; decay constant; trap depth; rare earths

Rare earth activated inorganic phosphors are widely used in a variety of applications, such as lamp industry, color display, radiation dosimetry and X-ray imaging. It is also known that Eu^{2+}-activated alkaline earth aluminates act as photoluminescent phosphors for their high quantum efficiency in the visible region as indicated in the investigations on the $MAl_2O_4:Eu^{2+}$ and $MAl_{12}O_{19}:Eu^{2+}$ (M=Ca, Sr, or Ba) phases described by Blasse et al.[1]. The luminescent properties of Eu^{2+}-doped strontium aluminates phosphors have been extensively studied since they show the long anomalous phosphorescence or the short-time decay depending on the conditions of preparation. Abbruscato[2] investigated afterglow and electrical properties of $SrAl_2O_4:Eu^{2+}$ (SAE), and proposed that holes are trapped at lattice defects. The study also demonstrated that Eu^{2+} emission is associated with the process of thermal de-trap.

Afterward, Eu^{2+}- and Dy^{3+}-coactivated strontium aluminates were developed[3,4], and they exhibited longer persistent phosphorescence than that of traditional sulfide- based ZnS:Cu,Co phosphors. Based on the investigations into the afterglow, thermoluminescence (TL), and photoconductivity characteristics of polycrystalline $SrAl_2O_4:Eu^{2+},Dy^{3+}$ (SAED), Matsuzawa et al.[5] suggested that the phosphorescence is ascribed to the presence of holes and to the trapping, as well as thermal release of holes by Dy^{3+} ions in the system. However, Qiu et al.[6] proved no evidence for valence conversion of Eu^{2+} to Eu^{+} and Dy^{3+} to Dy^{4+} after X-ray irradiation from X-ray absorption spectra in SAED. Therefore, they proposed that Eu^{2+} and Dy^{3+} ions do not directly act as holes and electron traps.

Takasaki et al.[7] investigated the afterglow characteristics of Eu^{2+} and Dy^{3+} co-doped $SrAl_2O_4$, and found the existence of at least two traps which were demonstrated by the glow curves of TL. The afterglow mechanism of SAED was studied by Ohta et al.[8] on the basis of afterglow (AG), photoluminescence (PL), and TL measurements via UV or X-ray irradiation. The trapping levels and kinetics parameter in SAED were investigated[9,10]. With the presumption of the hole-trap, the Sr defect was increasingly stabilized by a charge compensation upon doping Dy^{3+}. An electron trap probably originates from oxygen defects, which are produced by heating in the reductive atmosphere. Recently, the roles of co-activator of Eu^{2+}, Dy^{3+} in strontium aluminates have been studied with thermoluminescence spectrum by Deng et al.[11].

The synthesis of $SrAl_2O_4:Eu^{2+},Dy^{3+}$ phosphors by adding boron oxide as a high temperature flux tends to accelerate grain growth. The role of boron oxide has been reported in

Foundation item: Project supported by Industrial Technology Research Institute

Corresponding authors: I-Cherng Chen, Shiu-Shiung Lin (**E-mail:** eugenechen@itri.org.tw, glasgow1993@yahoo.com; **Tel.:** +886-6-3847045, +886-7-7317123 ext. 8291)

DOI: 10.1016/S1002-0721(12)60163-X

literature[12–15]. Chen et al. [14] have demonstrated a convenient sol-gel route leading to the formation of SAED phosphor with long afterglow property. They found that boron added into the synthetic reaction of SAED not only acts as a flux but also enhances the phosphorescent intensity. It also inclines to lengthen the afterglow duration[15]. Besides, the two afterglow peaks observed in boron-added SAED (BSAED) can probably be attributed to the presence of at least two types of traps.

In this paper, we reported the trap depths of different reduction routes of Eu^{3+} to Eu^{2+} and boron addition in SAED host to enhance the thermoluminescence, which is related to phosphorescent decay properties. We investigated the kinetics parameters of afterglow twin peaks of BSAED with optical filter separation. This was demonstrated by proving that the composition of two peaks is related to the Eu^{2+} luminescence centers distributed in miscellaneous strontium borate or strontium aluminates phases. It also confirmed that BSAED exhibited various strengths of crystal fields or different Eu^{2+} coordination environments. In addition to investigating thermoluminescence profiles, afterglow spectra and afterglow decay rates, we calculated the trap depths of SAED, BSAED, and SAE without Dy^{3+} co-doping phases from the Hoogenstraaten's plot of glow curves. Meanwhile, by keeping the same readout time for all specimens, we also applied commercial LumiNova® BG-300M as a reference measurement in this study.

1 Experimental

1.1 Samples preparation

Eu^{2+} and Dy^{3+}-coactivated $SrAl_2O_4$ phosphors were synthesized by sol-gel method without fluxes, and the detailed procedures of preparing the solution I and solution II had been reported[14]. Briefly, the solution I was prepared by dissolving 10 g of aluminum isopropoxide (98%, Strem Chemicals) in 100 ml of 2-methoxyethanol (99%, Merck) by refluxing at 110 ºC for 1 h. The solution II was prepared by dissolving nitrates of Sr, Eu and Dy with stoichiometry of 1:0.05:0.05 (all 99.9%, Aldrich Chemicals) in a mixture of 2-methoxyethanol and deionized water in 50:50 (*v*/*v*) proportions. To avoid hydrolysis of cations alkoxides before mixing, 6.5 g ethyl acetoacetate (EAA) was added into the solution I as a chelating agent before the mixing procedures. They were then thoroughly stirred and kept in an ice bath to form the gels. The molal stoichiometry for synthesizing BSAED in this work was 1:2:0.05:0.05:0.3 for Sr:Al:Eu:Dy:$B(OEt)_3$. The resulting white gels were then dried at 80 to 120 ºC for 5 h. The gels were subsequently heated at the temperature between 500 and 1200 ºC for 10–24 h, and lastly they were chemically reduced at 1300 ºC under the H_2/N_2 (5%:95%) atmosphere for 1 h. The Eu^{2+}-activated phase SAE was also synthesized by the same method. In addition, the reduced atmosphere under N_2 for SAED and under air for BSAED at 1300 ºC was applied as a contrast. The preparation conditions for various SAE, SAED and BSAED samples are summarized in Table 1. The crystalline phases were identified by using a Mac Science model MXP-3 X-ray diffractometer (XRD).

Table 1 Composition and preparation of strontium aluminates phosphors

Samples	Composition	Preparation
SAE-H_2/N_2	$SrAl_2O_4:Eu_{0.05}$	Firing at 1300 ºC, 5 h reducing at 1300 ºC, 1 h in H_2/N_2 (5%:95%)
SAED-N_2	$SrAl_2O_4:Eu_{0.05},Dy_{0.05}$	Firing at 1300 ºC, 5 h heating at 1300 ºC, 1 h in N_2
SAED-H_2/N_2	$SrAl_2O_4:Eu_{0.05},Dy_{0.05}$	Firing at 1300 ºC, 5 h reducing at 1300 ºC, 1 h in H_2/N_2 (5%:95%)
BSAED-air	$SrAl_2O_4:Eu_{0.05},Dy_{0.05},B_{0.3}$	Firing at 1000 ºC, 5 h heating at 1300 ºC, 1 h in air
BSAED-H_2/N_2	$SrAl_2O_4:Eu_{0.05},Dy_{0.05},B_{0.3}$	Firing at 1000 ºC, 5 h reducing at 1300 ºC, 1 h in H_2/N_2
LumiNova® BG-300M	$Sr_4Al_{14}O_{25}$:Eu,Dy	Commercial product manufactured by Nemoto & Co. in Japan

1.2 Spectra measurements

1.2.1 Phosphorescent afterglow (AG) spectra The measurements of phosphorescence spectra were performed on a Shimadzu RF-5301PC spectrophotometer equipped with a 150 W Xenon lamp and a Hamamatsu R928 type photomultiplier as an excitation source and a detector, respectively. The phosphor powders were compacted into a cylindrical dish groove (10 mm×5 mm) of a holder, and were then transferred to the spectrophotometer. Prior to measurements, the samples were stored in a dark chamber for 8 h to avoid the interference from pre-activating light. The $SrAl_2O_4$:Eu,Dy samples were then irradiated with ultraviolet (λ=254 nm) for 300 s prior to measuring the phosphorescent decay profiles. The initial intensity of phosphorescence (I_o) was measured approximately 1 s after the excitation had been terminated. Moreover, the time-dependent phosphorescence intensity (I) was measured at the emission wavelength of 485±5 nm in a dark chamber without excitation source.

1.2.2 Thermoluminescence (TL) spectra The measurements of glow curves (T/L 7188 Littemore) were performed for 300 s at room temperature from 40 to 500 ºC at heating rates of 1–5 ºC/s after 10 s of pre-irradiation with UV (λ=254 nm). In order to study the samples of BSAED and LumiNova® BG-300M on the afterglow doublet peaking at λ_{em} of 404±1 nm and 483±2 nm of twin peaks, the measurements of glow curves were carried out in a Littemore system model T/L 7188 equipped with optical filters of UV 450 nm cut-off filter and UV 400±30 nm band-pass filter. The procedures were performed from 40 to 500 ºC at heating rates of 1–5 ºC/s after the samples were pre-irradiated with UV (λ=254 nm) for 300 s at room temperature.

2 Results and discussion

2.1 Phase analysis and microstructure investigations

The XRD profiles for SAED, BSAED, and LumiNova®

BG-300M are shown in Fig. 1. SAED presents blue greenish phosphorescence, and it is mainly composed of $SrAl_2O_4$ and minor contents of $SrAl_{12}O_{19}$, as indicated in Fig. 1(1). Furthermore, the BSAED phase exhibits the typical blue-green afterglow, and Fig. 1(2) reveals that it forms a poorly structured crystalline phase coexisting with small amount glassy phase of Sr-borates. In fact, our previous investigation showed that $SrAl_2O_4$ phase dominates in the products of synthetic reactions with the initiating Al/Sr ratio from 1.5 to 7, whereas the $SrAl_{12}O_{19}$ phase exists as a major phase in those with Al/Sr ratio ranging from 5 to 12 derived from the sol-gel method[14].

The SEM micrographs for as-prepared SAED, BSAED and LumiNova® BG-300M are shown in Fig. 2(a)–(c). Irregular spherical grains with size of several tenths of microns to several microns are observed in as-prepared addition-free SAED (Fig. 2(a)), whereas the boron-added BSAED (Fig. 2(b)) exhibits inconsistent rectangular grains with partial melting morphology. The grain boundaries observed in BSAED with partial melting character are barely unambiguously recognized. Similarly, the SEM micrograph of commercially available LumiNova® BG-300M in Fig. 3(c) presents irregular grain morphology and slightly partial melting character, which is almost identical to that observed in the SEM micrograph of BSAED (Fig. 2(b)). This partial melting character of BSAED can presumably be attributed to the formation of a layer of low-density borates floating on the surface of bulk reactants.

2.2 Afterglow property and decay rate

The comparisons of initial phosphorescence spectra of

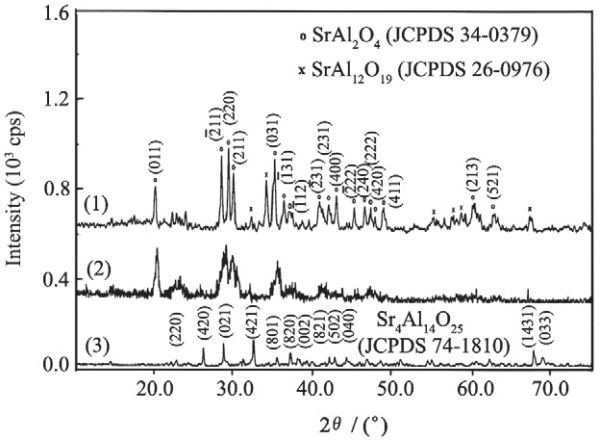

Fig. 1 XRD profiles for SAED (1), BSAED (2), and LumiNova® BG-300M (3) phases synthesized under various doping conditions

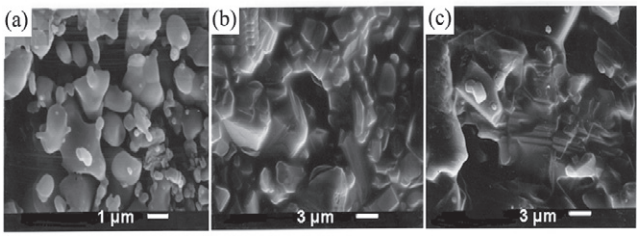

Fig. 2 Comparison of SEM microstructures for pristine and boron doped $SrAl_2O_4$:$Eu_{0.05}$,$Dy_{0.05}$ phases
(a) SAED; (b) BSAED; (c) LumiNova® BG-300M

BSAED-H_2/N_2, BSAED-air, SAED-H_2/N_2, SAED-N_2 and SAE-H_2/N_2 are shown in Fig. 3. The broad single or doublet emission bands peaking at different λ_{em}'s are attributed to the different environmental Eu^{2+} ions as the luminescent centers. Their typical $4f^65d^1 \rightarrow 4f^7$ transitions and the hole trap may be ascribed to the Sr^{2+} defects of host lattice that are believed to be stabilized by a charge compensation upon Dy^{3+} doping[19,20]. However, the observed λ_{em}'s for the five samples ranging from 483 to 500 nm are found to be shorter than that of the SAED phase at 520 nm reported by Matsuzawa et al.[5]. The observed discrepancy and shifting in the λ_{em}'s may probably be attributed to the difference in crystal field of Eu^{2+} inherited from the different preparation routes. The $4f^65d^1$ state is sensitive to crystal field[16–18]. It tends to split into sublevels depending on the strength of crystal field. The decreasing strength of crystal field from these sublevels inclines to make the luminescence vary in colors from red to blue. The doublet emission bands can be well observed in the samples of BSAED-H_2/N_2 and BSAED-air (Fig. 3(1), (2)).

Our previous study demonstrated that the role of boron-modification facilitates the formation of Eu^{2+}, and its presence has been proven to be substantial for $SrAl_2O_4$ phases to present longer phosphorescence characteristics[15]. The luminescent center of Eu^{2+} was proposed to be located in a loosening crystalline and non-homogeneous host environment with at least two types of coordination for boron-added SAED (BSAED). BSAED has been demonstrated in our study to potentially possess partial reduction of Eu^{3+} to Eu^{2+} even heated at 1300 ºC in the air. The host of boron-modified $SrAl_2O_4$ (BSAED) presents its structure as a heterogeneous composite that included major composition of $SrAl_2O_4$ and minor Sr-borates, which coexist in a complicated form of $SrO\text{-}B_2O_3$. A substitution defect model has been proposed by Pei et al.[19,20] that inequivalent substitutions of Eu^{3+} for Sr^{2+} tend to create electrons on Sr vacancies in Sr-borates. The tetrahedral BO_4 anion groups of compounds therefore act as electron transfer in the reduction process of Eu^{3+} to Eu^{2+}, and network of BO_4 tetrahedral may also perform as a shield to prevent oxygen diffusion.

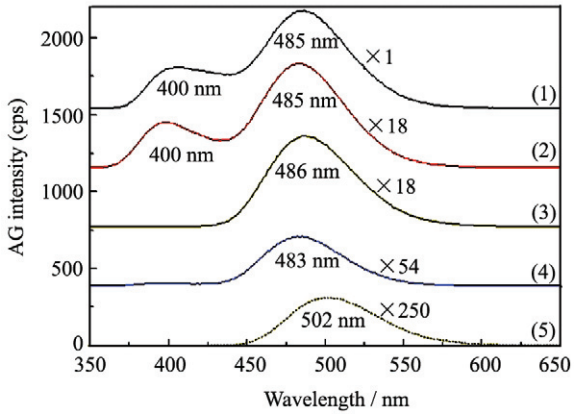

Fig. 3 Comparison of initial phosphorescence spectra for BSAED-H_2/N_2 (1), BSAED-air (2), SAED-H_2/N_2 (3), SAED-N_2 (4), and SAE-H_2/N_2 (5) (The measurement after irradiation with UV at λ=254 nm for 300 s at room temperature)

BSAED-H_2/N_2 (reduced in the H_2/N_2=5%:95% atmosphere) exhibits the strongest phosphorescence intensity and twin peaks among the five samples investigated in this report. Even the properties of BSAED-air heated in the air at 1300 ℃ are stronger than that of either SAED or SAE. On the contrary, the addition-free SAE phases show the weakest phosphorescence intensity (Fig. 3(5)). The observed enhancement of afterglow intensity due to boron addition is clearly found in BSAED-H_2/N_2 and BSAED-air, as compared to those of SAED and SAE (Fig. 3).

Regarding the time-dependent relative afterglow intensity (Fig. 4), the boron-free SAED-N_2 (reduced in the N_2 atmosphere, Fig. 4(4)) and the SAE-H_2/N_2 without co-doping of Dy^{3+} (Fig. 4(5)) exhibit the weakest intensity and the fastest decay rate. Nevertheless, the boron-added BSAED-H_2/N_2 (reduced in the 5%:95% of H_2/N_2 atmosphere, Fig. 4(1)) presents the strongest intensity, yet the slowest decay rate among the six samples in this study.

2.3 Thermoluminescence investigation

Thermoluminescence is a good way to detect the combination emission caused by thermal de-trapping of carriers. The energy corresponding to the glow peak is equal to the trap depth. What has to be emphasized is that traps and carriers (electrons and holes) may be produced by irradiation, but they are also to be created during sample processing. In order to understand the characteristics of the trapping centers in thermoluminescence, the reduced routes for BSAED, SAED and SAE were investigated accordingly. The profiles of glow curves (Fig. 5) were examined with plotting TL intensity against temperature for SAED specimens (Table 1). These specimens are derived from a sol-gel process which has been systematically assessed with thermal activation in different atmospheres. The TL profiles of Fig. 5(a)–(e) are respectively for SAE-H_2/N_2, SAED-N_2, SAED-H_2/N_2, BSAED-air and BSAED-H_2/N_2. These glow peaks indicate the existence of various traps with the different trap depths. The peak position of de-trapping temperature is directly correlated to the trap depths[21].

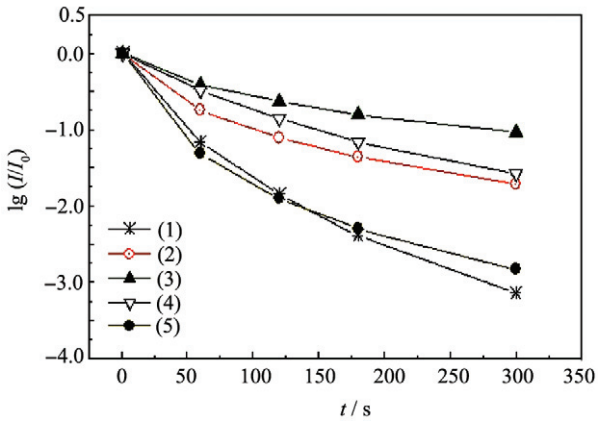

Fig. 4 Comparison of afterglow decay rates for SASED-N_2 (1), SAED-H_2/N_2 (2), BSAED-H_2/N_2 (3), BSAED-air (4), and SAE-H_2/N_2 (5) (The measurement after radiation with UV at λ=254 nm for 300 s at room temperature)

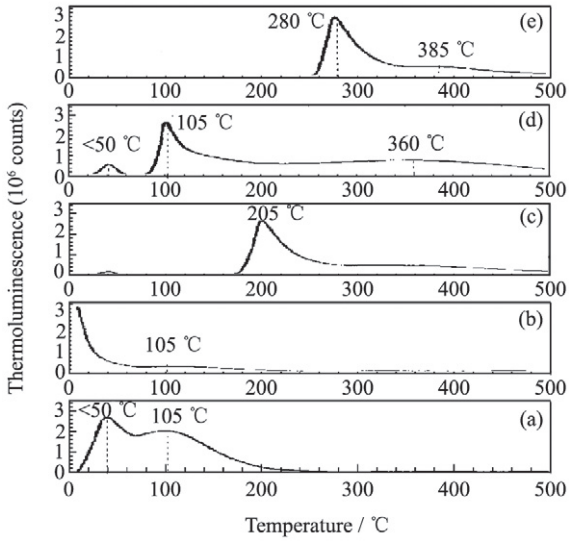

Fig. 5 Comparison of thermoluminescence profiles for SAE-H_2/N_2 (a), SAED-N_2 (b), SAED-H_2/N_2 (c), BSAED-air (d), and BSAED-H_2/N_2 (e) (The measurement of two-stage activation: 10 s of pre-irradiation followed with 300 s irradiation via UV at λ= 254 nm at room temperature)

It is interesting to note that the glow curves of SAE-H_2/N_2 (Fig. 5(a)), SAED-N_2 (Fig. 5(b)), and BSAED-air (Fig. 5(d)) possess two-peaking at 105 °C and around <50 °C. The samples of SAED-N_2 and BSAED-air are found to be very similar to SAE-H_2/N_2. In contrast, the reducing process of the H_2/N_2 atmosphere for SAED and BSAED significantly promotes the formation of deeper traps. Several thermal peaks are observed at 205 and 350 °C in SAED-H_2/N_2 (Fig. 5(c)), as well as at 280 and 385 °C in BSAED-H_2/N_2 (Fig. 5(e)). Furthermore, their ascribed common shallow traps are merely related to the existence of Eu^{2+} ions. However, the aid of the hole-trap effects with Dy^{3+} in SAED or BSAED hardly function for the reduction route of Eu^{3+} to Eu^{2+} in N_2 or in the air. The facilitating effect of Dy^{3+} only becomes efficient in the reduced H_2/N_2 atmosphere. The sequence of the trap depths in this study is ascribed as follows: SAE (without Dy^{3+} co-doping and boron-free)<SAED (boron-free)<BSAED. Besides, the similar broadened peaks are found at 375±10 °C for BSAED-H_2/N_2 and BSAED-air. It is therefore suggested that boron-modified $SrAl_2O_4$:Eu^{2+},Dy^{3+} shows deeper traps *in situ* than that of SAED which does not contain boron. Consequently it presents better afterglow properties compared to SAED in terms of phosphorescence intensity and persistent time.

Meanwhile, the time-dependent afterglow decay profiles during the first 5 min (between 0 and 300 s) for boron-added BSAED-H_2/N_2, and LumiNova® BG-300M ($Sr_4Al_{14}O_{25}$:Eu, Dy phase) are compared (Fig. 6). The maximum emission for boron-added BSAED-H_2/N_2 presents the doublet peaks at λ_{em} of 403 and 485 nm; similarly LumiNova® BG-300M possesses the doublet centering at λ_{em} of 400 and 482 nm (Fig. 6(a), (b)). The wavelengths of the afterglow peaks for BG-300M are found to be extremely close to those observed in BSAED-H_2/N_2. Furthermore, the relative intensity ratios

of the afterglow peaks at 400±1 nm for BSAED- H_2/N_2 and 486±4 nm for BG-300M, are found to change in a non-systematic fashion with time. This finding on the afterglow decay behaviors may suggest that the observed afterglow from twin peaks of BSAED-H_2/N_2 and BG-300M may be rationalized by considering the contributions from at least two types of hole or electron traps with different trap energy in the boron added phases or simply from different aluminates or borates containing Eu^{2+}. For the two peaks of BG-300M samples, we infer the condition proposed by Smets et al.[22,23] that Sr^{2+} in the $Sr_4Al_{14}O_{25}$ exhibits two positions of an equal number of lattices. Therefore the occurrence of Eu^{2+} to replace Sr^{2+} presents the equal probability of the two locations, and the two emission peaks appeared at the wavelengths of 490 and 410 nm. Since the corresponding absorption spectrum of the two large areas overlapping may enhance energy shifting from the short wavelength of 410 nm to the long wavelength of 490 nm[24], the differentials tend to appear between the main peak and weaker peak respectively at 490 and 410 nm. In order to study the findings on the afterglow decay behaviors, each emission peak of TL (λ=400±1 nm and 486±4 nm) with optical filter separation for BSAED-H_2/N_2 and LumiNova® BG-300M were evaluated (Fig. 7(a), (b)). The thermal peaks are observed at 250 °C (λ=400 nm) and 280 °C (λ=483 nm) for BSAED-H_2/N_2, also at 260 °C (λ=400 nm) and 280 °C (λ=490 nm) for BG-300M. The difference of thermal peaks for BSAED-H_2/N_2 is 40 °C higher than 20 °C of BG-300M. Furthermore, the non-exponential afterglow decay rate of individual peaks (λ=400±1 nm and 486±4 nm) for BSAED-H_2/N_2 and BG-300M are investigated (Fig. 6).

The features of different decay rates in different time periods for all the afterglow decay curves (Fig. 8) obviously indicate the presence of various types of traps with the different depths in the samples. The reduced afterglow decay rate derived from the plot of lg I/I_0 versus time (Fig. 8) was assessed. And the sequence of decay rate is revealed as follows: (λ=400 nm of BG-300M)>(λ=400 nm of BSAED-H_2/N_2)>(λ=485 nm of BG-300M)>(λ=485 nm of BSAED-H_2/N_2). It is suggested that the observed afterglow from twin peaks of BSAED-H_2/N_2 and BG-300M, may be rationalized by considering the contributions from at least two types of hole or electron traps with different trap energy in the boron-added phases, or simply from different aluminates or borates containing Eu^{2+}.

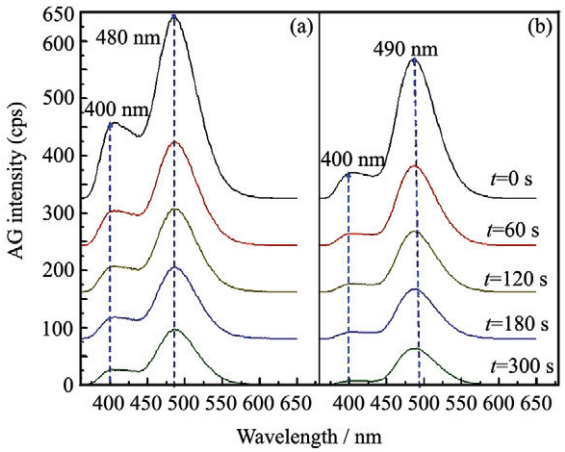

Fig. 6 Comparison of time-dependent afterglow decay profiles for BSAED-H_2/N_2 (a) and Nemoto BG-300M (b) (The measurement after irradiation with UV at λ=254 nm for 300 s at room temperature)

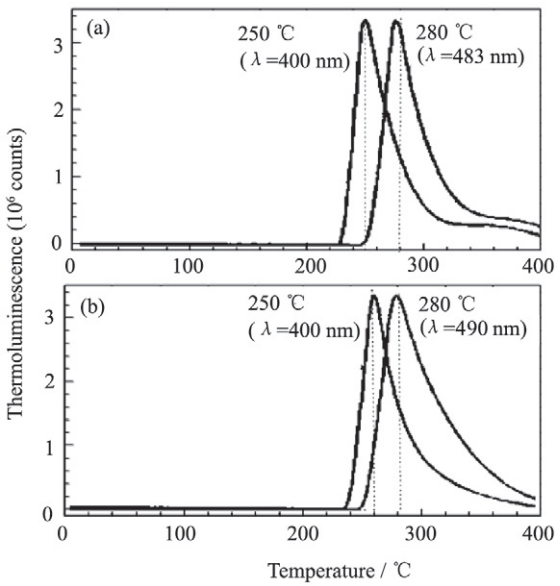

Fig. 7 TL glow curves of separating twin peaks for BSAED-H_2/N_2, (a) and Nemoto BG-300M (b) samples measured with a heating rate of 1.5 ºC/s (The measurement of two-stage activation: 10 s of pre-irradiation followed with 300 s irradiation via UV at λ= 254 nm at room temperature)

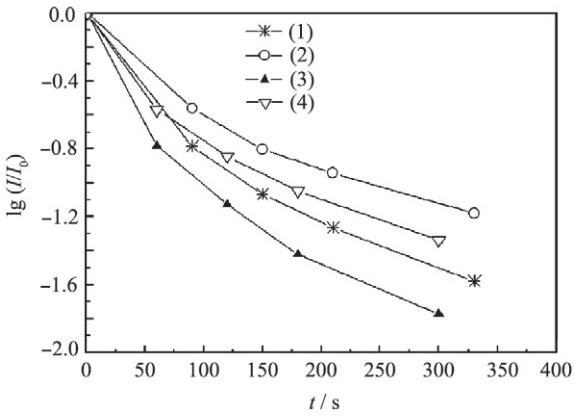

Fig. 8 Comparison of afterglow decay rates for separating twin peaks of BSAED-H_2/N_2 (peak at 400 nm) (a), BSAED-H_2/N_2 (peak at 480 nm) (b), BG-300M (peak at 400 nm) (c), and BG-300M (peak at 490 nm) (d) (The measurement of two-stage activation: 10 s of pre-irradiation followed with 300 s irradiation via UV at λ=254 nm at room temperature)

2.4 Calculation of traps depth and decay constant

Investigations into the thermoluminescence profiles, afterglow spectra and afterglow decay rates have enabled us to calculate the trap depths of SAED, BSAED and without Dy^{3+} co-doping of $SrAl_2O_4$:Eu^{2+} (SAE) phases. The data were derived from the Hoogenstraaten's plot of glow curves.

The depth of traps in the specimens was obtained by analyzing glow-peak shape, heating rate and glow peak of TL curves. The Hoogenstraaten's method was applied to measure the glow curves with various heating rates β shown in different peak positions Tm, by using the following equation:

$$\ln[\beta/Tm^2]=-\varepsilon/k[1/Tm]+\ln[sk/\varepsilon] \quad (1)$$

where s is the frequency factor, and k is the Boltzmann constant. The trap depth ε is determined by the plot of $\ln(\beta/Tm^2)$ against $1/Tm$[25].

The Hoogenstraaten's plots for SAED-H_2/N_2, SAE-H_2/N_2, BSAED-H_2/N_2 and BG-300M are presented in Fig. 9. The depths of energy trap based on the Hoogenstraaten's plot of afterglow curves are summarized in Table 2. The afterglow spectrum shows twin-peak of both BSAED-H_2/N_2 and BG-300M at 400±1 nm and 486±4 nm, which are two individuals composed and contributed from the different depths of traps. They are 0.57 and 0.76 eV for BSAED-H_2/N_2, as well as 0.59 and 0.72 eV for Nemoto BG-300M. The depths of the traps are determined to be 0.43 and 0.18 eV, for SAED and SAE, respectively. The calculations of trap depths are reasonable in comparison with those reported by Takasaki et al.[7] (i.e. trap 1=0.26 eV, trap 2=0.55 eV; ranging from 0.37 to 0.64 eV) and Ohta et al.[8] (i.e. 0.82 and 0.75 eV). In this study, the measurement of phosphorescent decay profiles shows data acquisition of samples to fit well by bi-exponential functions in 300 s. The decay equation is described as:

$$I(t)=A\exp(-\lambda_1 t)+B\exp(-\lambda_2 t) \quad (2)$$

where I is afterglow intensity, t is time, A and B are constants, λ_1 and λ_2 are decay constants.

The afterglow measurements are fitting the decay equation for samples of SAED, SAE and BSAED, which are assessed via different reduction routes of Eu^{3+} to Eu^{2+} in $SrAl_2O_4$ hosts. The commercial LumiNova® BG-300M has been applied as a contrast (Fig. 4(1)–(5)). The afterglow twin peaks of both BSAED-H_2/N_2 and BG-300M are centered at 400±1 nm and 486±4 nm, which are two individual decay behaviors (Fig. 8). The calculated results of decay constant for afterglow peaks of samples are presented as a quantitative form regarding decay behaviors of $SrAl_2O_4$ specimens (Table 3). The results shown in Table 3 illustrate that the specimens hold a better afterglow property with the sequence of: SAE-H_2/N_2>SAED-N_2>SAED-H_2/N_2>BSAED-air>BG-300M>BSAED-H_2/N_2.

Besides, the observations of afterglow decay behaviors and TL glow curves in this study appear to indicate the different modes of trapping mechanisms. Regarding boron-added, Dy^{3+}co-doped and different reduction routes of Eu^{3+} to Eu^{2+}, they can be attributed to the presence of hole and/or electron traps with different depths. The Dy^{3+} co-doped in $SrAl_2O_4$:Eu^{2+} plays a role of stabilizing and increasing Sr defects, and consequently it tends to aid the formation of hole traps[8]. It is well demonstrated that $SrAl_2O_4$:Eu^{2+} (SAE-H_2/N_2) without Dy^{3+} co-doping only presents the poor afterglow in terms of intensity and decay rate (Fig. 3(5); Fig. 4(e)), even with its possession of the lowest trap depth among all samples. Meanwhile, boron added into the synthetic reaction of $SrAl_2O_4$:Eu,Dy (BSAED) not only acts as a flux but also enhances the phosphorescent intensity (Fig. 3(1), (2)). And it tends to lengthen the afterglow duration as well (Fig. 4(a), (b)). As to the addition of B_2O_3 in $SrAl_2O_4$:Eu,Dy host, the manipulation possesses several functions, including to promote the reduction of Eu^{3+} to Eu^{2+}, to lower the concentration quenching effect of Eu^{2+}, and to increase defects to give rise *in situ* to the deeper traps, which are proved with TL (Fig. 5(d), (e)). The afterglow twin peaks of BSAED compose two individual peaks (Fig. 3(a), (b)). They are related to the Eu^{2+} luminescence centers distributed in

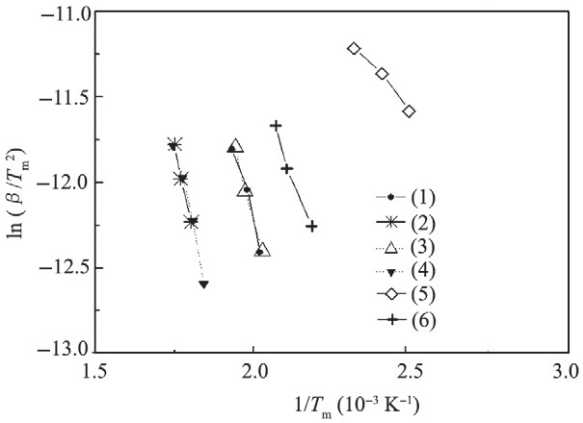

Fig. 9 Hoogenstraaten's plots of glow peaks for BSAED-H_2/N_2 (peak at 400 nm) (1), BSAED-H_2/N_2 (peak at 480 nm) (2), BG-300M (3) (peak at 400 nm), BG-300M (peak at 490 nm) (4), SAE-H_2/N_2 (5), and SAED-H_2/N_2 (6) (The measurement of two-stage activation: 10 s of pre-irradiation followed with 300 s irradiation via UV at λ=254 nm at room temperature)

Table 2 Trap depth relevant to the long afterglow of strontium aluminates phosphors

Samples	Composition	E trap depth/eV
BSAED	$SrAl_2O_4$:$Eu_{0.05}$,$Dy_{0.05}$,$B_{0.3}$	P_1=0.59 eV (peak at 400 nm)
		P_2=0.76 eV (peak at 485 nm)
SAED	$SrAl_2O_4$:$Eu_{0.05}$,$Dy_{0.05}$	0.43 eV
SAE	$SrAl_2O_4$:$Eu_{0.05}$	0.18 eV
LumiNova®	$Sr_4Al_{14}O_{25}$:Eu,Dy	P_1=0.57 eV (peak at 400 nm)
BG-300M	(commercial product)	P_2=0.72 eV (peak at 490 nm)

Table 3 Comparison of decay constants during the initial stage of AG decay (first 300 s)*

Samples	λ_1/s^{-1}	λ_1/s^{-2}	Main peak position/nm
(a) SAE-H_2/N_2	22	3.1	502
(b) SAED-N_2	19.3	7.0	483
(c) SAED-H_2/N_2	12.5	3.3	486
(d) BSAED air	8.1	4.0	485
(e) BSAED-H_2/N_2	6.5	2.2	485
(f) LumiNova® BG-300M	2.5	2.7	490

* $T(t)=T_{cr}\exp(-\lambda_1 t)$; λ_1: decay constant; The decay behaviors can be best fitted by the following decay equation with two exponential terms; Decay equation: $I(T_f)=A\exp(-\lambda f_t)+B\exp(-\lambda_2 t)$)

miscellaneous phases and different defect traps, and this is verified by TL (Fig. 7(a)) and decay behaviors (Fig. 8(a), (b)) with optical separation. Besides, the hole trapping effect of Dy^{3+} has operated under the H_2/N_2 reduced atmosphere, which is ascribed to raising more electron trap of oxygen defects to assist afterglow mechanism in $SrAl_2O_4:Eu^{2+},Dy^{3+}$ host (Fig. 5). The details in the mechanism of the afterglow will require further studies in the future.

3 Conclusions

The effect of the thermoluminescence and afterglow properties of $SrAl_2O_4:Eu^{2+},Dy^{3+}$(SAED) and boron-modified SAED (BSAED) phases were associated with the heating procedure in different reduction atmospheres by sol-gel process. The addition of boron aided reduction routes of Eu^{3+} to Eu^{2+} in $SrAl_2O_4:Dy^{3+}$ host that was related to phosphorescent decay properties. BSAED showed the deeper traps *in situ* than that of SAED which contains no boron. And it was accordingly better than SAED in terms of afterglow properties. The function of Dy^{3+} enhanced the hole-trapping effect, and it required both SAED and BSAED to be heated at 1300 °C high temperature under H_2/N_2 (5%:95%) atmosphere. The calculations of the trap depth energy and decay constant were corresponding to the measurement results of thermoluminescence and afterglow decay curves.

References:

[1] Blasse G, Bril A. Fluorescence of Eu^{2+} activated alkaline-earth aluminates. *Philips Research Reports*, 1968, **23**: 201.

[2] Abbruscato V. Optical and electrical properties of $SrAl_2O_4:Eu^{2+}$. *Journal of the Electrochemical Society*, 1971, **118**: 930.

[3] Royce Martin R, Tamaki H, Murazaki Y. Long decay phosphors. U. S. Patent 5, 376, 303. 1994.

[4] Murayama Y, Takeuchi N, Aoki Y, Matsuzawa T. Phosphorescent phosphor. U.S. Patent 5, 424, 006. 1995.

[5] Matsuzawa T, Aoki Y, Takeuchi N, Murayama Y. A new long phosphorescent phosphor with high brightness $SrAl_2O_4:Eu^{2+}$, Dy^{3+}. *Journal of the Electrochemical Society*, 1996, **143**: 2670.

[6] Qiu J, Kawasaki M, Tanaka K, Shimizugawa Y, Hirao K. Phenomenon and mechanism of long lasting phosphorescence in Eu^{2+}-doped aluminosilicate glasses. *Journal of the Physics and Chemistry of Solids*, 1998, **59**: 1521.

[7] Takasaki H, Tanabe S, Hanada T. Long-lasting afterglowcharacteristics of Eu, Dy co-doped SrO-Al_2O_3 phosphor. *Journal of the Ceramic Society of Japan*, 1996, **104**: 322.

[8] Ohta M, Maruyama M, Hayakawa T, Nishijo T. Role of dopant on long-lasting phosphor of strontium aluminate. *Journal of the Ceramic Society of Japan*, 2000, **108**: 284.

[9] Arellano-Tánori O, Meléndrez R, Pedroza-Montero M, Castañeda B, Chernov V, Yen W M, Barboza-Flores M. Persistent luminescence dosimetric properties of UV-irradiated $SrAl_2O_4:Eu^{2+},Dy^{3+}$ phosphors. *Journal of Luminescence*, 2008, **128**: 173.

[10] Chernov V, Meléndrez R, Pedroza-Montero M, Yen W M, Barboza-Flores M. The behavior of thermally and optically stimulated luminescence of $SrAl_2O_4:Eu^{2+},Dy^{3+}$ long persistent phosphor after blue light illumination. *Radiation Measurements*, 2008, **43**: 241.

[11] Deng L Y, Hu Y H, Wang Y H, Wu H Y, Xie W. Afterglow and thermoluminescence spectrum of $SrAl_2O_4:Eu^{2+}$ and $SrAl_2O_4:Eu^{2+},Dy^{3+}$. *Chinese Journal of Quantum Electronics* (in Chin.), 2010, **27**(3): 257.

[12] Chang Y L, Hsiang H I, Liang M T. Effect of B_2O_3 addition on formation and luminescence of the $SrAl_2O_4:Eu^{2+},Dy^{3+}$ phosphor prepared using solid state reactions. *Journal of Alloys and Compounds*, 2008, **461**: 598.

[13] Nag A, Kutty T R N. Role of B_2O_3 on the phase stability and long phosphorescence of $SrAl_2O_4$:Eu,Dy. *Journal of Alloys and Compounds*, 2003, **354**: 221.

[14] Chen I C, Chen T M. Effect of host compositions on the afterglow properties of phosphorescent strontium aluminate phosphors derived from the sol-gel method. *Journal of Materials Research*, 2001, **16**: 1293.

[15] Chen I C, Chen T M. Sol-gel synthesis and the effect of boron addition on the phosphorescent properties of $SrAl_2O_4:Eu^{2+}$, Dy^{3+} phosphor. *Journal of Materials Research*, 2001, **16**: 644.

[16] Sun J Y, Shi C S, Li Y M. The influence of crystal-field and covalent characteristic on the electronic transition emission of Eu^{2+}(II). *Chinese Science Bulletin*, 1989, **34**: 703.

[17] Qiu J, Miura K, Sugimoto N, Hirao K. Preparation and fluorescence properties of fluoroaluminate glasses containing Eu^{2+} ions. *Journal of Non-Crystalline Solids*, 1997, **213&214**: 266.

[18] Ju S H, Kim S G, Choi J C, Park H L, Mho S I, Kim T W. Determination of the solid solubility of $SrAl_2O_4$ in $CaAl_2O_4$ through crystal field-dependent Eu^{2+} signatures. *Materials Research Bulletin*, 1999, **34**: 1905.

[19] Pei Z, Zeng Q, Su Q. The application and a substitution defect model for Eu^{3+} to Eu^{2+} reduction in non-reducing atmospheres in borates containing BO_4 anion groups. *J. Phys. Chem. Solids*, 2000, **61**: 9.

[20] Machida K, Adachi G, Shiokawa J. Luminescence properties of Eu(II)-borates and Eu^{2+}-activated Sr-borates. *Journal of Luminescence*, 1979, **21**: 101.

[21] McKeever S W S. Thermoluminescence of Solids. New York: Cambridge University Press, 1988. 64.

[22] Smets B M J. Phosphors based on rare-earths, a new era in fluorescent lighting. *Materials Chemistry and Physics*, 1987, **16**: 283.

[23] Smets B, Rutten J, Hoeks G, Verlijsdonk J. $2SrO{\cdot}3Al_2O_3:Eu^{2+}$ and $1.29(Ba,Ca)O{\cdot}6Al_2O_3:Eu^{2+}$ two new blue-emitting phosphors. *Journal of the Electrochemical Society*, 1989, **136**: 2119.

[24] Blasse G. Energy transfer between inequivalent Eu^{2+} ions. *Journal of Solid State Chemistry*, 1986, **62**: 207.

[25] Hoogenstraaten W. Electron traps in ZnS phosphor. *Philips Research Reports*, 1958, **13**: 515.